Experimental characterization of an asymmetric valveless pump based on soft robotics technology

J. Anatol, M. García-Díaz, C. Barrios-Collado, J. A. Moneo-Fernández, F. Castro-Ruiz, J. Sierra-Pallares[1]

AFFILIATIONS

Departamento de Ingeniería Energética y Fluidomecánica & ITAP, Universidad de Valladolid, Paseo del Cauce 59, 47011 Valladolid, Spain

ABSTRACT

Asymmetric pumping can be achieved by periodically compressing a flexible tube in its plane of symmetry using an actuator, as long as the rigid pipes connected to its ends are asymmetric. This mechanism, together with impedance pumping, compose the Liebau effect. While there have been numerous studies on impedance pumping, there is a lack of available research on asymmetric pumping. The aim of this study is to examine the influence of key parameters on the performance of this type of pump. In addition, this study implements an actuator based on soft robotics technology in asymmetric valveless pumping for the first time. The pump developed in this study can be applied in different areas involving the pumping of special fluids, including biomedical applications.

I. INTRODUCTION

In many applications (e.g., biomedical engineering), it is necessary to pump fluids without coming into contact with them. One option is to use so-called valveless pumping, the most well-known types of which are peristalsis and the Liebau phenomenon[1]. Valveless pumping based on the Liebau effect[2] works via the periodic pinching of a flexible element (a compliant tube) with an asymmetry in the pincher position, the circuit, or a combination of both[3–5]. Unlike peristaltic pumps, the direction of net flow and its magnitude depend nonlinearly on the pinching frequency and duty cycle[6,7]. Under certain pinching frequencies, a Liebau pump can show a reverse flow direction [8,9]. In addition, Liebau-effect pumps can achieve the same performance as peristaltic pumps, but with the advantage that only a small portion of the flexible tube contracts, unlike in peristalsis, where the entire length of the flexible tube must be in active contraction [10].

Since its discovery in the mid-20th century, numerous studies have described the mechanism of the Liebau pump, a mechanically simple device with a dynamically complex mechanism[11–15]. The practical applications of the Liebau pump are diverse, from cardiovascular assistance to cooling in electronics. The clinical use of biocompatible Liebau pumps to drive fluid flow in different parts of the body has also been discussed[16,17]. In other areas, the commercial viability of Liebau pumps for use in cooling high-performance electronic systems has been demonstrated[18].

Anatol et al.[4] described the two pumping effects that occur in the Liebau phenomenon, shown in Fig. 1, which have previously been observed[8]. Impedance pumping occurs when the pincher is not in the symmetry plane of the compliant tube, and the pressure waves are reflected with a phase lag in the impedance change zones between the rigid and flexible tube. This effect creates a pressure field that produces the pumping, as seen in Fig. 1(b). Otherwise, if the pincher is located in the plane of symmetry of the compliant tube, the reflected waves at its ends cancel

[1] Corresponding author: jsierra@uva.es

each other out, and the asymmetric hydraulic resistance terms at each end of the compliant tube (length, diameter, material) generate pumping due to the phase shifts of the waves traveling in the circuit, as seen in Fig. 1(c).

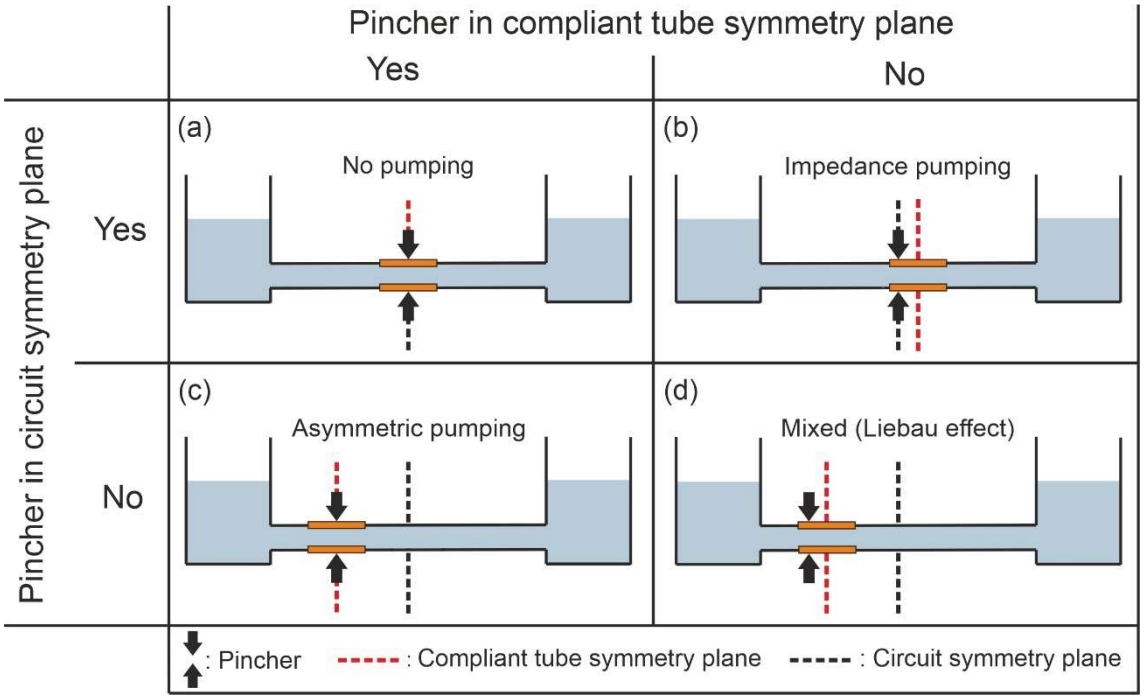

Figure 1. Impedance and asymmetric pumping illustrating asymmetry through length of compliant tubing. (a) No pumping system, (b) impedance pumping, (c) asymmetric pumping, and (d) a mixed system (Liebau effect).

The core of a Liebau pump is a flexible compliant tube and the pinching mechanism that deforms it. The pinching mechanism consists of an actuator that compresses the compliant tube, referred to as the pincher. Different types of pinchers have been used, such as a piston, a flat pincher, a diaphragm, and a ring. The pinching mechanism can be based on piezoelectric[18], electromagnetic[19], pneumatic[4], artificial skeletal muscle[20], and even biologically compatible materials[21].

Among the valveless pumping phenomena based on the Liebau effect, asymmetric pumping has been studied considerably less than impedance pumping. Among the most outstanding authors are Tagaki and Saijo, who experimentally studied this type of pumping in 1983. They built a circuit comprising a horizontal pipe joining two reservoirs with a piston operating at a point on the horizontal pipe not equidistant from both reservoirs. The results were theoretically verified using a mathematical model that considered the relationships between the flow rate, time, pressure, and pinching frequency[22]. Later, in 1985, Tagaki and Takahashi carried out another analytical and experimental study of the circuit, but this time with pressurized reservoirs, and obtained more specific information about the resonant frequency of the system, which allowed optimization of the pump performance[23].

Further experimental studies on asymmetric pumping are to be found in the work of Anatol et al.[4], in which the effectiveness of asymmetric pumping was analyzed from changes in the pinching frequency and characteristics of the compliant tube. A higher flow rate was pumped with frequencies close to the resonant frequency. In this work, we follow this line of research in order to shed more light on this type of valveless pumping.

The theoretical background of asymmetric pumping was described by Propst[24] using a period-averaged mechanical energy equation. In that research, a system similar to the one described in Fig. 1(c) was analyzed theoretically. It was shown that the pumping is caused by the difference in kinetic energy between the two branches, as was also pointed out by Avrahami and Gharib[25]. Propst also found that the difference in the phase average levels of the reservoirs is proportional to the difference in kinetic energy between the two branches. Jung and Kim[26] established that the optimum frequency for working with asymmetric pumps is the resonant frequency, at which phase synchronization in time between the fluid pressure difference and the external pinching force is obtained, thus enabling energy storage in the discharge reservoir.

To our knowledge, this study proposes for the first time the use of a soft robot as a pincher in asymmetric pumping. Soft robots are currently emerging as a highly viable option in applications in which finesse and malleability are required. By using specifically engineered soft structures, soft robots can be made to produce different types of movements: extension, contraction, bending, and twisting. Furthermore, being air-driven and made of silicone, they are a very good alternative for biocompatible devices[27,28].

This type of pump could be used in extracorporeal blood pumping in medical therapies such as extracorporeal membrane oxygenation (ECMO)[29], dialysis, and plasmapheresis. The Liebau pump eliminates the need for blades or recirculating zones, minimizing hemolysis and thrombus formation, which are blood disorders that affect overall survival outcomes.

The pump proposed in this study consists of a compliant tube connected to rigid pipes at its ends. A soft robot designed as a silicone ring and used as a pincher periodically compresses the compliant tube in its central position. The soft-robotic pincher is robust, easy to manufacture, produces significant pumping for biological applications, and can be easily scaled if necessary.

This paper aims to study the mechanism of asymmetric pumping in depth. The temporal evolution of the flow rates and instantaneous pressures are studied throughout. The performance and operation of the innovative soft robotic pincher are analyzed in terms of its duty cycle, operating pressure, and pinching frequency. In addition, the performance of the pincher used in this paper is compared with a mechanical pincher used in previous studies. Finally, a parametric study of key variables in asymmetric pumping without valves is carried out to deduce the best working conditions of the pump.

II. MATERIALS AND METHODS

A. Experimental test rig

An experimental test rig was built for hydraulic characterization of the asymmetric pump. A diagram is shown in Fig. 2. It consisted of two identical cross-section reservoirs connected by two rigid PVC pipes of different lengths (length ratio $\lambda = L_2/L_1$), which were joined by a flexible tube constructed by the authors[4] [4]. This was used as a compliant tube into which the soft robot is placed to act as a pincher. The PVC pipes were easily interchangeable so that circuit configurations of different length ratios could be established. To carry out tests under stable conditions, the two reservoirs were connected by means of a silicone pipe fitted with a gate valve, called a return pipe. Water was used as the working fluid, with the density $\rho = 1000$ kg m^{-3} and viscosity $\mu = 0.001$ kg m^{-1} s^{-1} kept constant throughout the experiments.

The instrumentation consisted of three pressure meters (Keller PD-23, Switzerland) and four unidirectional ultrasonic flowmeters (Sonotec Sonoflow CO.55/239H V2.0, Germany). Two of

the three pressure meters, P1 and P2, were located on both sides of the compliant tube, as shown in Fig. 2. The remaining pressure meter Pd was placed at Reservoir 2 to measure the water level in this reservoir. The flowmeters, arranged in pairs — F1-F2 on rigid pipe 1 and F3-F4 on rigid pipe 2 — allowed measurement of the instantaneous flow rate and its direction in both pipes. Flow rates were considered positive when directed from Reservoir 1 to Reservoir 2. The pressure and flow meter uncertainties were 4% and 2%, respectively.

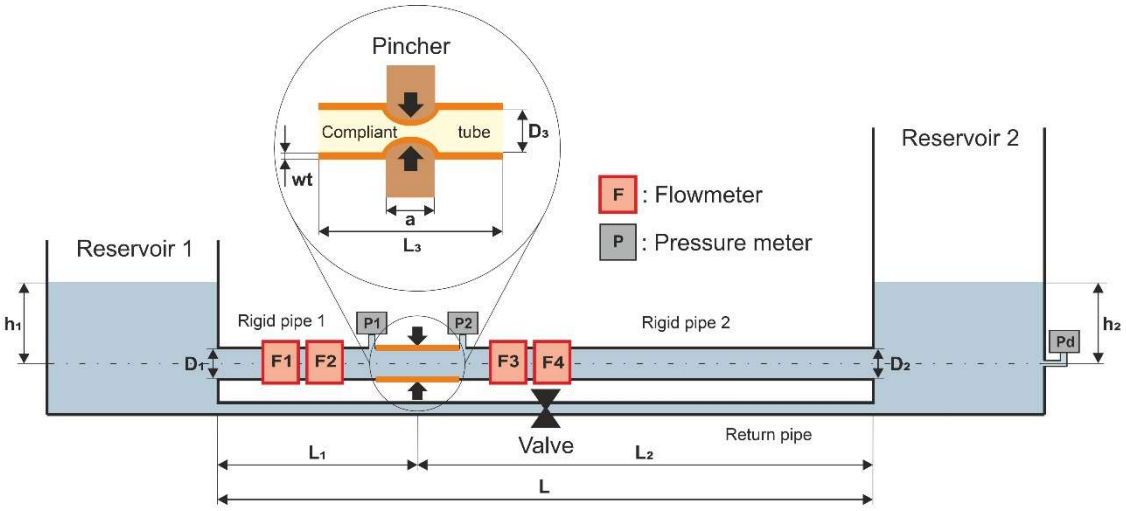

Figure 2. A schematic diagram of the asymmetric pumping test rig with an illustrative subpanel showing the enlarged compliant tube being compressed by the pincher.

For comparison with previous studies, the test rig was configured with the same parameters as those in Anatol et al.[4], called the nominal parameters. The nominal geometric parameters are shown in Table 1. Tests performed with nominal values of the parameters are said to be under nominal conditions.

Table 1. Nominal values of the geometric parameters.

Parameter	h_1	h_2	D_1	D_2	D_3	a
Nominal value	40 cm	40 cm	16 mm	16 mm	20 mm	20 mm

Parameter	L	L_1	L_2	L_3	wt	λ	K
Nominal value	400 cm	75 cm	325 cm	10 cm	0.7 mm	4.33	20%

1. Soft robotic pincher

The pincher was based on soft robotics technology and was designed to eliminate the moving parts that existed in our previous mechanical pincher, making it smaller and more biocompatible[4] [4]. The pincher is a silicone ring with a hollow chamber inside, the dimensions of which are shown in Fig. 3(a). The ring is placed inside a rigid outer shell made of PLA, which holds the soft robot in position, as seen in Fig. 3(b). The ring design allows it to deform only on the side facing the compliant tube. This deformation compresses the compliant tube of the asymmetric pump, creating the pumping action. The pincher is pneumatically driven by compressed air at a nominal gauge operating pressure of P_t = 1.4 bar. The compressed air supply was designed with four radially symmetric inlets to make the pressure uniform in the inner chamber and reduce the kinetic energy dissipation of the compressed air at the inlet, as seen in Fig. 3(a). The soft robot's opened (top) and closed (bottom) positions when inflated with

compressed air are shown in Fig. 3(b). This closure resulted in a quasi-circular seal around the compliant tube.

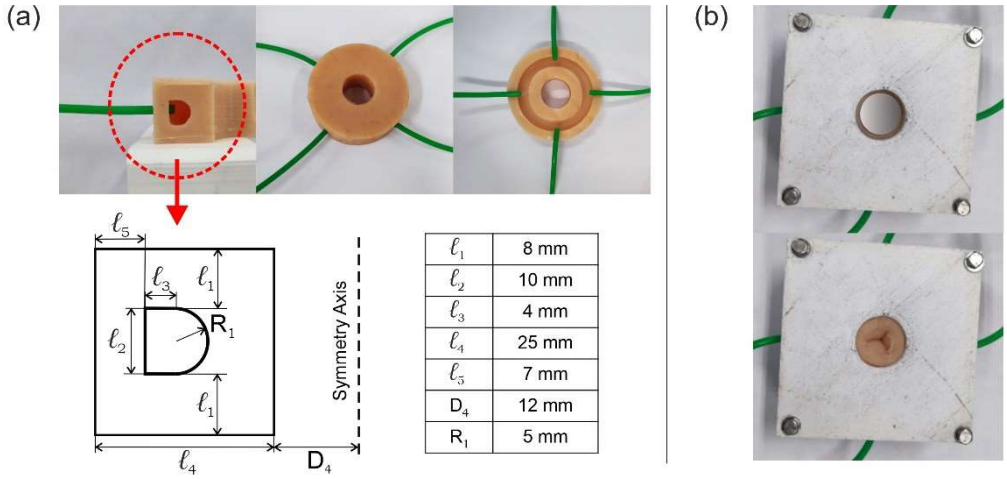

Figure 3. The silicone ring based on soft robotic technology. (a) The soft robot with compressed air inlets in its inner chamber and ring dimensions. (b) The soft robot open and closed in its rigid outer shell.

The soft robot was made by molding with Easyplat 00-30 platinum silicone (Feroca, Spain), which made the device biocompatible. The molding process of the soft robot is detailed in Fig. 4. All the molds used were made of PLA using a FDM 3D printer. First, the lower part of the device was molded by placing mold B in mold A. Mold B provided the shape of the inner chamber. Once the silicone had hardened, the inner piece, mold B, was removed. Mold A was mounted onto mold C, and the upper part of the soft robot was molded, completing the soft robot.

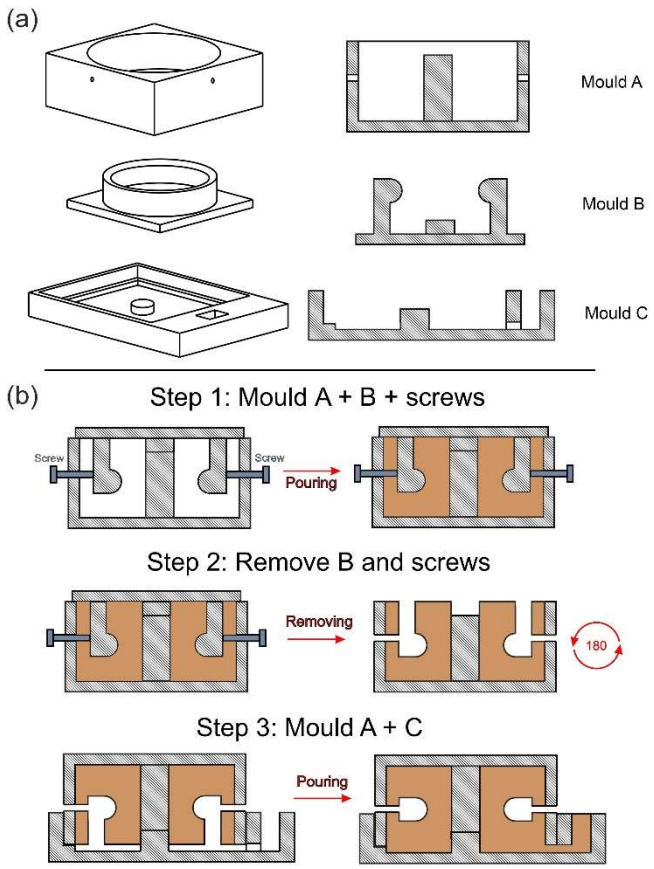

Figure 4. (a) Molds for producing the soft robotic pincher and (b) the steps of the molding process.

2. Control and measurement systems

The operating cycle of the soft robot has two phases. In the first, the compressed air entering the soft robot causes it to expand and compress the compliant tube (pincher closed, PC). In the second, the compressed air is discharged, and the compliant tube is released (pincher open, PO). The control system enables the compression time to be changed as a percentage of the cycle time. This percentage is called the duty cycle[11,30] and is defined in Eq. (1). The nominal duty cycle is 33%.

$$Duty\ cycle = \frac{PC}{PC+PO} \quad \text{(Eq. 1)}$$

There are two options for setting the pinching frequency (the inverse of the cycle period) at which the soft robot compresses the compliant tube: the first option, called manual frequency, is to set a specific pinching frequency, which remains unchanged during the test. In the second option, known as automatic frequency, the control system determines the resonant frequency and readjusts it after each cycle, because the resonant frequency evolves during unsteady experiments. For steady tests, the resonant frequency is constant even if the automatic frequency mode is established.

The control system is based on Arduino Nano®. The resonant frequency is determined from the signal of the instantaneous flow rate flowing through rigid pipe 1, as in the system used to control our previous mechanical pincher[4]. This resonant period corresponds to the time

between two consecutive peaks of the positive instantaneous flow rate at the junction of rigid pipe 1 and the compliant tube.

The data acquisition system was based on an Arduino Due® board that recorded the instantaneous values measured by the instruments with an adjustable time resolution, typically 1 ms.

B. Methodology and testing

Two types of tests were performed. The first type, known as steady tests, consists of having the two reservoirs connected by the return pipe. In this configuration, the pump operates at a single working point. Under these conditions, a study was made of the instantaneous flow rates in each of the pipes and the evolution of the pressure at the ends of the compliant tube. A frequency sweep was performed to analyze their relationship with the net flow rate (Q_{NET}) that was pumped. The influence of geometric parameters on the net pumped flow rate was observed, and finally, the influence of the duty cycle and the operating pressure on the net pumped flow rate was studied.

In the second type of test, known as unsteady tests, the reservoir return pipe is closed. This way, it is possible to see the time evolution of the pump through all its operating points, from the maximum net flow rate to the maximum head. The initial condition is that the reservoirs have the same water level. The temporal evolution of the net flow rate and the difference in head between the reservoirs ($H = h_2 - h_1$) are recorded until the maximum head is reached.

The maximum net flow rate obtained in the unsteady tests occurs at t = 0, when pumping starts and the heads in both reservoirs are equal. These tests make it possible to obtain the pump characteristic curves for comparison with the characteristic curves of the mechanical diaphragm pincher, in order to analyze the influence of different parameters on the maximum head achieved.

For setting the pinching frequency, the tests can be carried out in automatic or manual frequency mode. The mode in each test is indicated together with the results. Finally, the tests can be carried out under nominal conditions or by varying the parameter values, and this choice is also specified in the results section. We consider the nominal conditions to be the geometric parameters listed in Table 1 and the operating parameters of the soft robot: the operating pressure $P_t = 1.4$ bar and the duty cycle of 33%.

The data were processed and analyzed with MATLAB®. The head and net flow rate were time-averaged in each operating cycle. For steady tests, the maximum dispersion of the Q_{NET} data was close to 5%, which is in the range of the reported flowmeter uncertainty (4%). For unsteady tests, we observed a similar data dispersion below 4.7%.

III. RESULTS

A. Instantaneous flow rate evolution

A steady test was carried out in the automatic frequency mode. Each of the rigid pipes was fitted with a pair of unidirectional flowmeters to record the instantaneous flow rate in both directions, that is, either toward the reservoirs or toward the compliant tube. Flow rates were considered

positive when moving toward Reservoir 2. Flow rate 1 (Q_1) is the instantaneous flow rate through rigid pipe 1 and flow rate 2 (Q_2) is that through rigid pipe 2.

Figure 5 shows the evolution of the instantaneous flow rate in both rigid pipes under nominal conditions, using the phase average calculated from data from 121 consecutive operating cycles. The data dispersion was below 5%. The energy transmitted by the soft robot when the pincher is closing causes the fluid to be propelled toward the reservoirs from the midpoint of the compliant tube, which corresponds to the shaded part in Fig. 5. Subsequently, the water returns to refill the compliant tube, an effect shown on the non-shaded side of the same figure (PO). This phenomenon forms two opposing wave patterns of different amplitudes, with the Q_1 amplitude being greater because rigid pipe 1 has a lower hydraulic resistance. The net flow rate is obtained from the difference between the positive and negative parts of the instantaneous flow rate in either of the two curves. The maxima of the instantaneous flow rates are much larger than the resulting net flow rate.

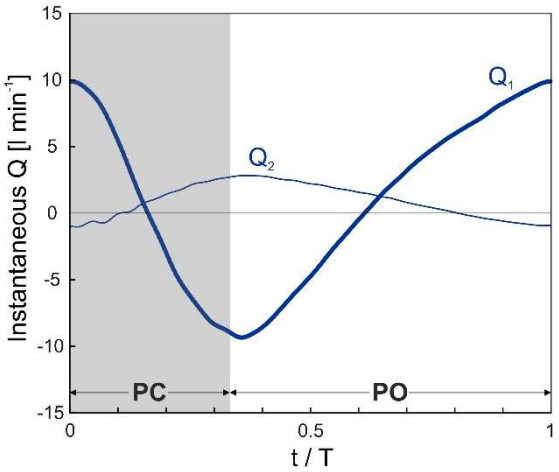

Figure 5. The evolution of instantaneous flow rates in the rigid pipes under nominal conditions and steady tests during a period (T). Q_1: The phase-averaged instantaneous flow rate in rigid pipe 1, Q_2: The phase-averaged instantaneous flow rate in rigid pipe 2. The pincher is closed for 33% of T. The phase averages are calculated from data from 121 consecutive operating cycles.

For nominal conditions, the net flow rate obtained was 2.5 l min^{-1}, which corresponds to a Reynolds number of 3300. The Womersley number, based on Eq. (2), varied between 6 and 20 depending on pinching frequency.

$$\mathrm{Wo} = r\sqrt{\frac{\rho f}{\mu}}\ , \qquad \text{(Eq. 2)}$$

where *r, ρ, f,* and μ are vessel radius, fluid density, pinching frequency, and fluid dynamic viscosity, respectively.

B. Pressure evolution

To determine the time evolution of the pressures, instantaneous gauge pressure records were obtained at both ends of the compliant tube. Figure 6 shows the time evolution of the pressures at P1 and P2 in a steady test with the automatic frequency mode. The data shown in Fig. 6(b)

was obtained in a test under nominal conditions. The other two data sets shown in Figs. 6(a) and 6(c) were obtained under non-nominal conditions by changing the length ratio.

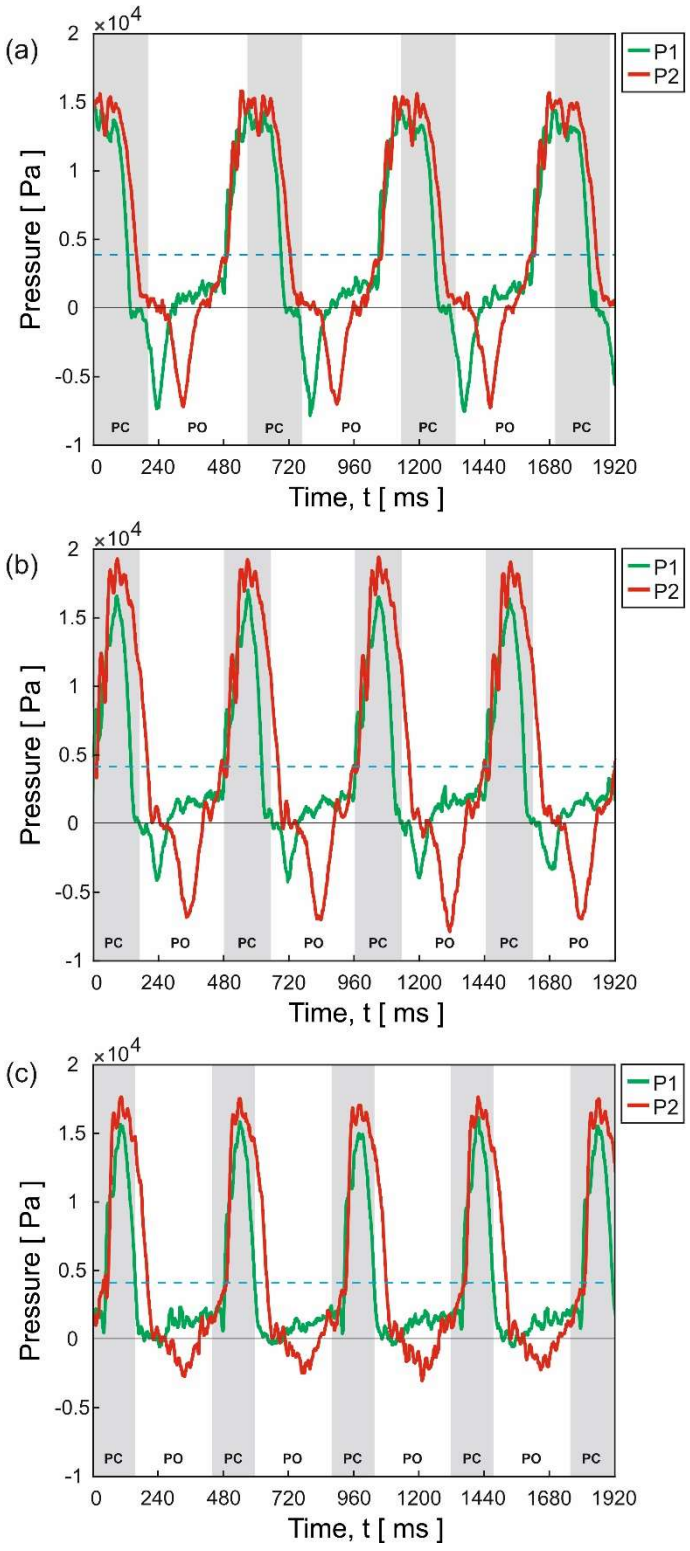

Figure 6. The evolution of the instantaneous pressure at the ends of the compliant tube in a steady test for three different length ratios (λ). The pincher is closed for 33% of T. The transmural pressure = 3923 Pa (dashed blue line). (a) λ=2.5, (b) λ=4.33 (nominal conditions), (c) λ=5.

Figures 6(a), 6(b), and 6(c) have in common that positive pressure peaks appear when the pincher compresses the compliant tube and the pressure waves propagate toward the ends of the compliant tube, where they are recorded by P1 and P2.

These peaks are in phase due to the symmetric position of the pincher with respect to the ends of the compliant tube. The difference in amplitude of the positive peaks is the result of the asymmetry in the length of the rigid pipe in the circuit at the two ends of the compliant tube. This asymmetry, defined by the length ratio (λ), determines the behavior of the pressure waves throughout the cycle. After the sudden increase in pressure caused by the closing of the pincher (PC), a pressure decrease in P2 undergoes an offset with respect to P1 due to the difference in the lengths of the pipes. This causes a different flow rate distribution. Therefore, the pressure decrease is observed sooner in the case of the pipe with the higher flow rate. The evolution of the maximum pressure value coincides with that of the net flow rate: the higher the pressure, the greater the instantaneous flow rate, and consequently, the greater the net flow rate.

When the pincher pushes the fluid toward the reservoirs, a depression zone is created in the compliant tube, as the kinetic energy increases in accordance with the mechanical energy balance. As λ increases, L_1 decreases and L_2 increases (the total length $L = L_1 + L_2$ is constant), as does the fluid mass inside them and, therefore, their inertia. The shorter the length of L_1, the shorter the period of the flow rate wave, and the sooner it fills the compliant tube and damps the depression. P1 is damped more than P2 because it is closer to Reservoir 1. For $\lambda = 5$, the pressure is fully damped, as seen in Fig. 6(c). Therefore, the minimum pressure value decreases with λ. The pinching frequency is closely related to the dynamics of rigid pipe 1, as it is the one that refills the compliant tube. A higher λ means a shorter L_1, leading to shorter refill times of the compliant tube and therefore a higher frequency.

C. Soft robotics pincher analysis

The performance of our soft robotic pincher is defined by three parameters: the pinching frequency, the duty cycle, and the pressure of the compressed air that drives it, called the operating pressure (P_t). A series of tests were carried out to characterize the operation of the pincher and to analyze the performance according to these parameters. The ranges of the parameters shown in the results are those allowed by the working limitations of the pincher.

1. Pinching frequency

Figure 7 shows the net flow rate obtained from a steady test in the system for different pinching frequencies under nominal parameters. These frequencies were fixed manually for each of the tests. Highly non-linear behavior of the net flow rate with the pinching frequency is observed. The maximum net flow rates are obtained at the resonant frequency, with negative net flow rates obtained (toward Reservoir 1) for frequencies a long way from the resonant frequency.

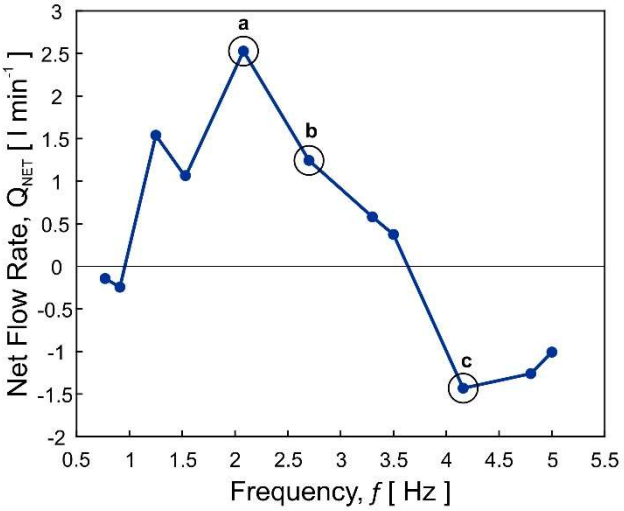

*Figure 7. Net flow rates for different pinching frequencies under nominal conditions in a steady test. Points **a**, **b**, and **c** are analyzed in detail in Fig. 8.*

When the pinching frequency is the resonant frequency (point **a** in Fig. 7), the pumped flow is at a maximum and in the expected direction. For frequencies close to the resonant frequency, positive net flow rates are obtained but they are not as high. When we move away from the resonant frequency, the pumping is reversed due to the high degree of mismatch between the pinching frequency and the system's natural frequency. In order to understand the appearance of negative net flow rates when working at certain pinching frequencies, Fig. 8 shows the evolution of the instantaneous flow rate (Q_1) together with the operating cycle for the values highlighted in Fig. 7.

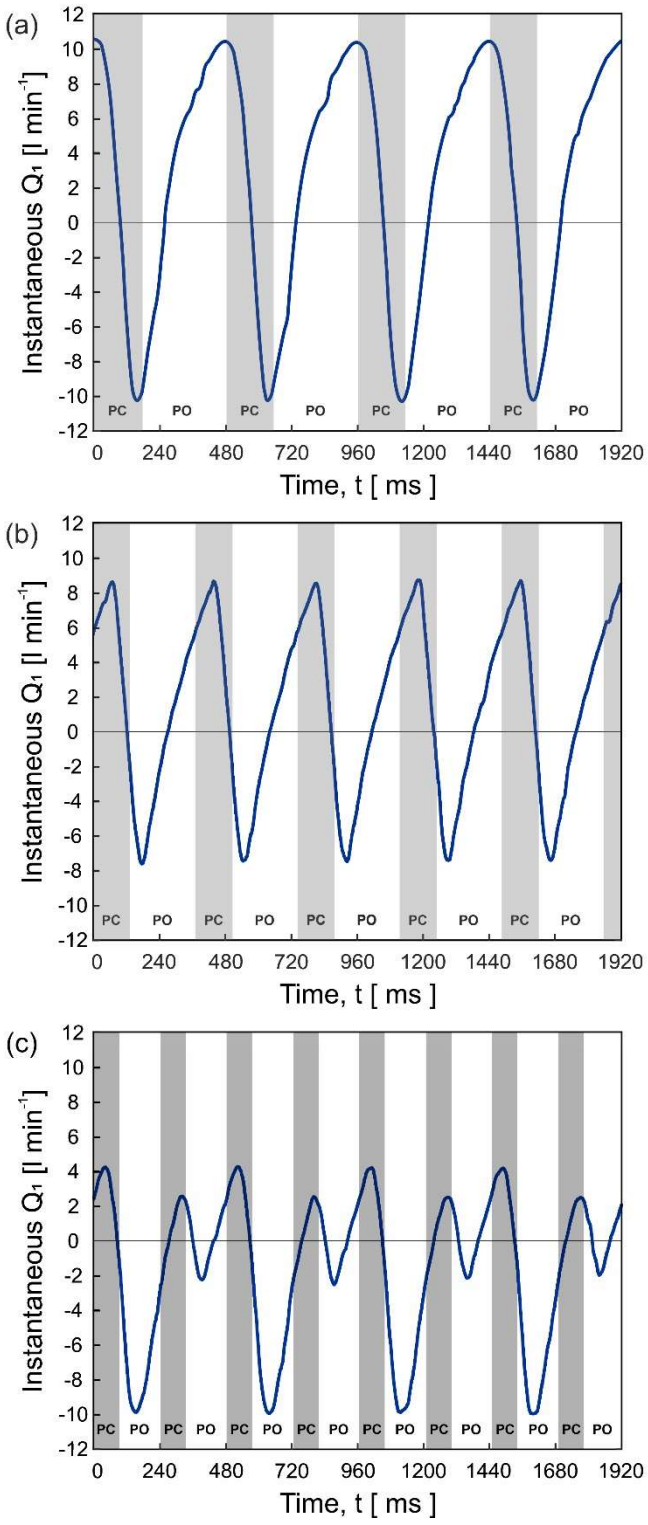

Figure 8. Instantaneous flow rates in rigid pipe 1 (Q_1) for different pinching frequencies under nominal conditions in a steady test. (a) $f = f_R = 2.08$ Hz (maximum positive net flow rate), (b) $f = 2.7$ Hz (positive net flow rate), (c) $f = 4.16$ Hz (negative net flow rate).

Figure 8(a) shows the case for the resonant frequency. Here, the pincher closure is in phase with the flow rate wave arriving at the compliant tube. This frequency corresponds to the natural frequency of the system. Figure 8(b) shows the case for a slightly different frequency from the resonant frequency. In this case, pinching occurs before the flow wave reaches its maximum, so

the compliant tube is unable to recover its resting volume and the net and instantaneous flow rates are therefore diminished. Figure 8(c) shows the case for a frequency at a distance from the resonant frequency, which results in the net flow rate being negative. The pinching frequency is so high that the filling of the compliant tube from rigid pipe 1 is blocked, causing Reservoir 2 to rise, which results in a negative net flow rate.

2. Duty cycle and operating pressure effect

Figure 9 shows the net flow rate obtained for different duty cycles as a function of the operating pressure (P_t), which is the pressure of the compressed air driving the pincher. A series of steady tests were performed in the automatic frequency mode. As the operating pressure and duty cycle changed, the only nominal values that remained the same were the geometric ones.

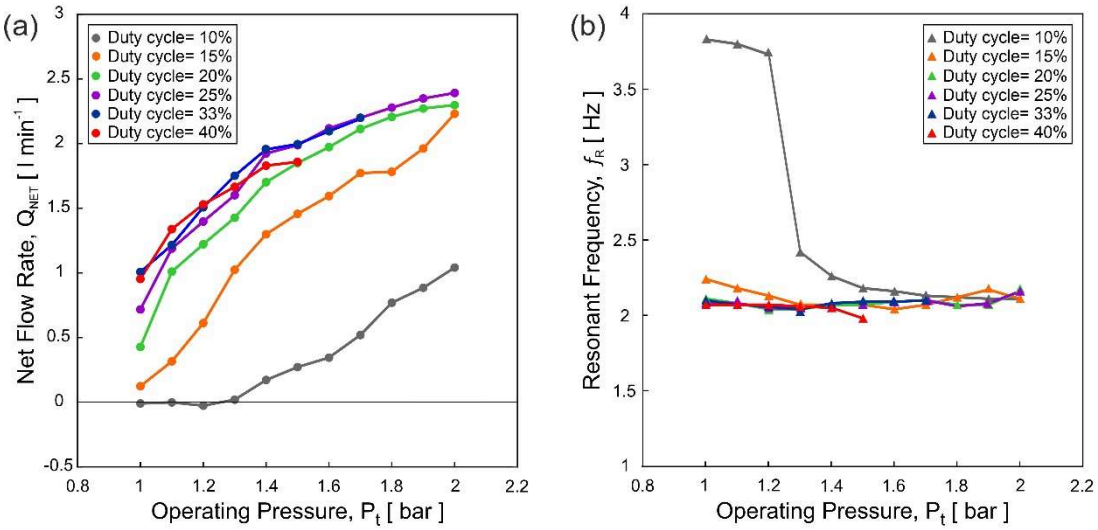

Figure 9. The evolution and variation of the (a) net flow rate and (b) resonant frequency with the duty cycle and operating pressure in a steady test. (For the geometric nominal parameters, see Table 1.)

Higher compressed air pressure results in a higher closing speed of the soft robot when compressing the compliant tube. This in turn leads to an increased instantaneous peak flow rate and, therefore, to a greater kinetic energy difference between the branches. As a result, there is a higher net flow rate through the test rig. This trend is observed for the entire duty cycle range, as seen in Fig. 9(a).

Meanwhile, as the duty cycle is increased with the pressure fixed, the net flow rate increases. This is due to the fact that the augmented closing time allows greater deformation of the compliant tube, displacing more liquid volume. There is a maximum point when working with a duty cycle of 33% at all pressures, after which an increase in this does not generate higher flow rates. This would indicate that from a duty cycle of 33% upwards, almost complete closure of the soft robot is achieved. Thus, keeping the soft robot closed for a longer period once it has reached its maximum closure does not help to generate an additional net flow rate. The additional time that the pincher remains closed interrupts the return of water to the compliant tube, which is not long enough for it to recover its original volume before the next closure. Consequently, the maximum instantaneous flow rate is reduced.

Figure 9(b) shows the resonant frequency for the different duty cycles and operating pressures under study. In the area corresponding to the duty cycles where the soft robot can close the

compliant tube completely (duty cycle greater than 15%), all the frequencies converge to a very similar value. This is defined as the resonant frequency of the system because it is totally independent of the pincher parameters (the operating pressure and duty cycle). The resonant frequency is therefore dependent solely on the geometric parameters of the test rig.

D. Performance Curves

In order to characterize the asymmetric pumping, it is necessary to define what is part of the asymmetric pump. In this study, the asymmetric pump is defined as the set of two reservoirs and three pipes, i.e., the two rigid pipes together with the compliant tube and the soft robotic pincher. The rationale behind this definition is that any variation of these parameters influences the pump performance curves.

We evaluate the energy consumed by the soft robotic pincher in each cycle, considering that it expands only by fully compressing the compliant tube. The whole process is isothermal, so mass forces and kinetic energy can be neglected. The energy consumed per cycle can be calculated from the enthalpy of the mass of compressed air entering the pincher,

$$\Delta\mathcal{H} = \Delta m\, h = \Delta m\, c_p\, \theta = \frac{c_p}{R}\left(P\left(V_0 + \frac{\pi {D_4}^2}{4}\ \ell_2\right) - P_0\, V_0\right), \qquad \text{(Eq. 3)}$$

where $\mathcal{H}$, c_p, θ, m, R, P, P_0, V_0, D_4, and ℓ_2 are, respectively, the energy consumed (enthalpy), the specific heat at constant pressure, the temperature, the mass of air inside the pincher, the specific gas constant, the absolute supply and initial (atmospheric) pressures, the air initial volume, the inside diameter at rest, and the length of the inner chamber.

In the case of a mechanical pincher[4], pinching is achieved is by means of a double-acting piston fed at a gauge pressure of 4 bar. Considering that the piston has no dead volume, the energy per cycle can be calculated from

$$\Delta\mathcal{H} = 2\frac{c_p\, P\, \frac{\pi D^2}{4}\, s}{R}, \qquad \text{(Eq. 4)}$$

where D and s are, respectively, the diameter (1 cm) and the stroke of the piston (2.3 cm). The calculated energies per cycle for the soft robotic and mechanical pincher are, respectively, 9.056 and 6.34 J/cycle.

The drive power, W_d, is calculated as the product of the energy per cycle and the pinching frequency, f.

$$W_d = \Delta\mathcal{H}\, f \qquad \text{(Eq. 5)}$$

The efficiency, η, is calculated as the ratio of the power transmitted to the fluid to the drive power,

$$\eta = \frac{\rho\, g\, H\, Q}{W_d}, \qquad \text{(Eq. 6)}$$

where ρ, g, H, and Q are, respectively, the density of the fluid, the acceleration due to gravity, the difference in height of the reservoirs, and the flow rate.

The curves of the head in Fig. 10(a), the pumping power in Fig. 10(b), the efficiency in Fig. 10(c), and the drive power in Fig. 10(d) are shown versus the flow rate of the asymmetric pump for two pinchers: the soft robotic pincher shown in this study and the mechanical pincher developed in Ref.[4]. It is observed that the performance achieved with the soft robotic pincher is much

greater than that of the mechanical pincher. The performance curve is of a higher order of magnitude for the soft robot, indicating that it provides more effective power transfer.

The soft robot needs approximately half the compressed air pressure of the mechanical pincher in order to operate. This is mainly due to the absence of mechanical friction losses. However, the mass of air demanded is greater, and therefore energy consumption is 50% higher. Consequently, the energy consumption per cycle of the soft robot is higher than that of the mechanical pincher (9.056 and 6.34 J/cycle, respectively) at the optimum frequency, which, as expected, is very similar, at 1.69 Hz and 1.53 Hz. This results in a greater drive power of 15 W vs. 9 W. In both cases, the low rate of efficiency is due to the air volume requirements for driving the pinchers, which need a mass of stored compressed air that is later eliminated.

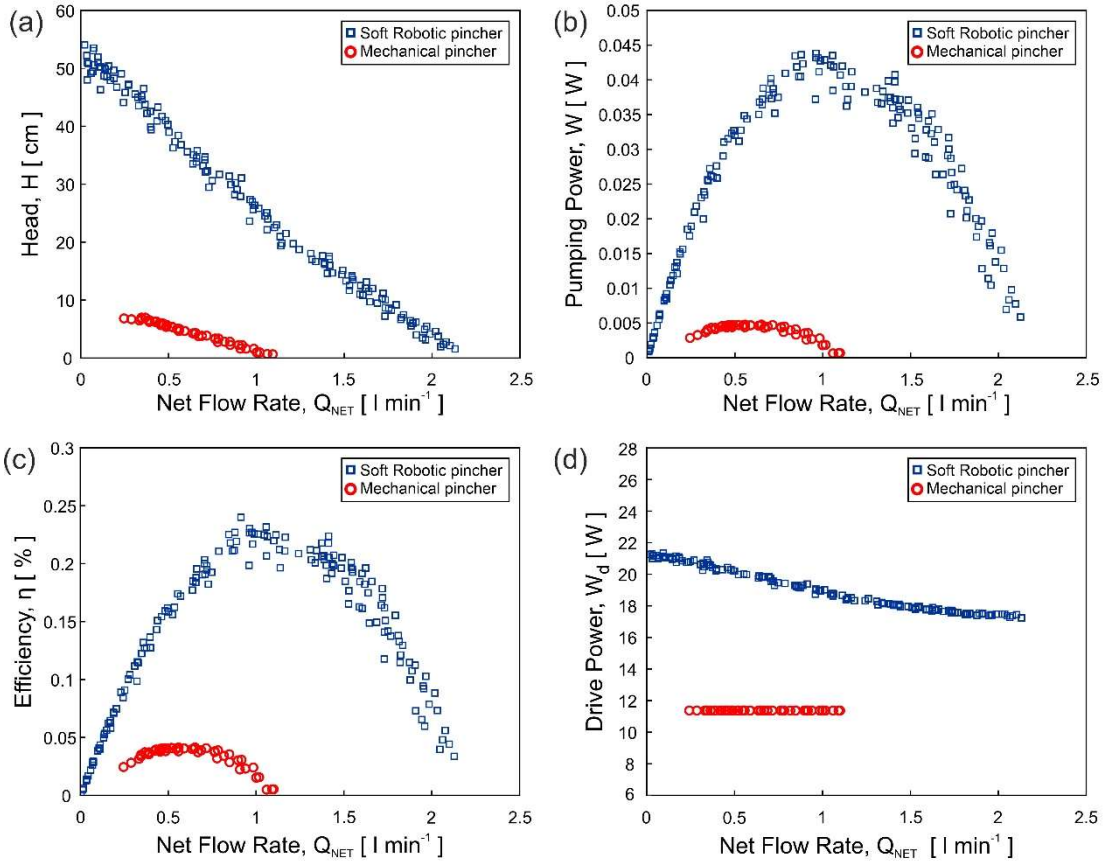

Figure 10. A comparison of the performance and characteristic curves of a soft robotic pincher and a mechanical pincher under nominal conditions in an unsteady test. (a) The pumping head, (b) the pumping power, (c) the efficiency, and (d) the drive power versus the net flow rate.

E. Parametric study

The test rig was designed to facilitate changing the geometric parameters and studying their influence on asymmetric pumping. Firstly, an analysis was performed of the influence of the length ratio (λ), which evaluates the level of length asymmetry in the pump. With the other parameters under nominal conditions, only the lengths of the rigid pipes L_1 and L_2 were modified, and the desired ratio was established at $L=L_1+L_2= 4$ m. The tests were carried out in automatic frequency mode, in both unsteady tests to analyze the maximum pumping head, and in steady tests to analyze the net flow rate. In terms of the maximum pumping head, there are two maxima for λ= 2 and λ= 4.5, as seen in Fig. 11(a). Figure 11(b) shows that the net flow rate

increases with the ratio λ until it reaches a maximum at λ= 4.5, after which it decreases. For λ= 1, symmetry exists in the hydraulic resistance and as expected, no pumping effect occurs. A ratio of λ= 5 cannot be exceeded due to the limitations of the rig.

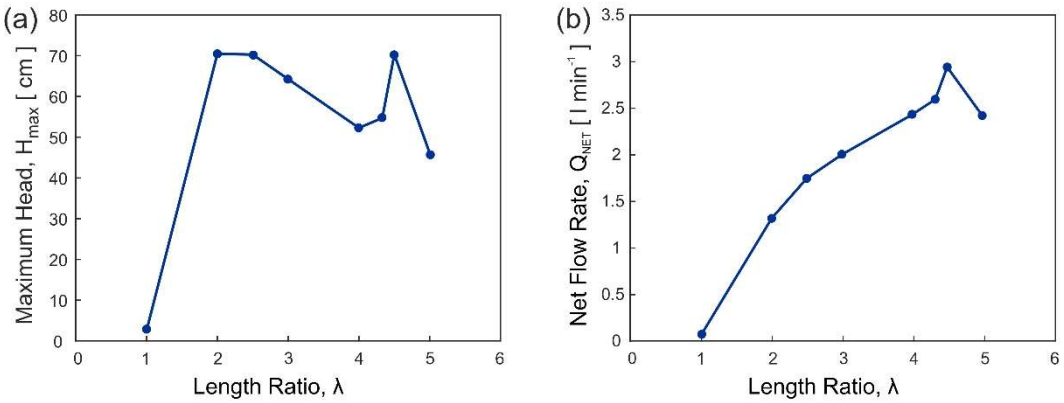

Figure 11. (a) The maximum pumping head in an unsteady test and (b) the net flow rate for different length ratios (λ) in a steady test (under nominal conditions).

Additionally, the frequency parameter f/f_R versus net flow rate was studied for different length ratios (λ) under steady conditions and in the manual frequency mode, in order to adjust the percentages of the resonant frequency (f_R). The non-linear evolution of the net flow rate with frequency was similar for all length ratio (λ) values. Maximum net flow rate values were observed for the resonant frequency for all length ratios, with the maximum being obtained for a ratio of 4.5, as seen in Fig. 12. For frequencies at a distance from the resonant frequency, and in terms of all length ratios, the net flow rate was negative (toward Reservoir 1).

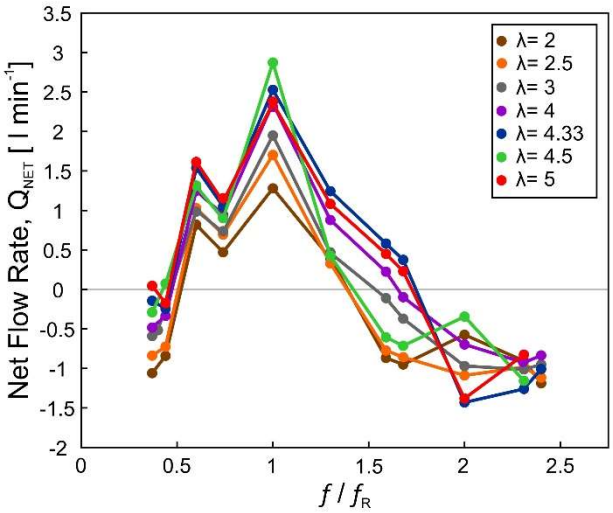

Figure 12. The net flow rate obtained for a frequency sweep covering different length ratios (λ) in steady tests (under nominal conditions).

Another parameter that was varied was the length of the compliant tube (L_3). All the other parameters were kept under nominal conditions and the automatic frequency mode was used. The results are shown as a function of the pinched tube length ratio (K) in Fig. 13.

In terms of the maximum head, better results were achieved with increasing K, as shown in Fig. 13(a). The net flow rate decreased slightly as K increased, as a greater length of the compliant tube was pinched, as shown in Fig. 13(b). The resonant frequency (f_R) increased with K, as seen in Fig. 13(c).

When the pinched tube length ratio is close to 50%, the proximity of the rigid pipes prevents the required deformation of the compliant tube. Under these conditions, performance is drastically reduced.

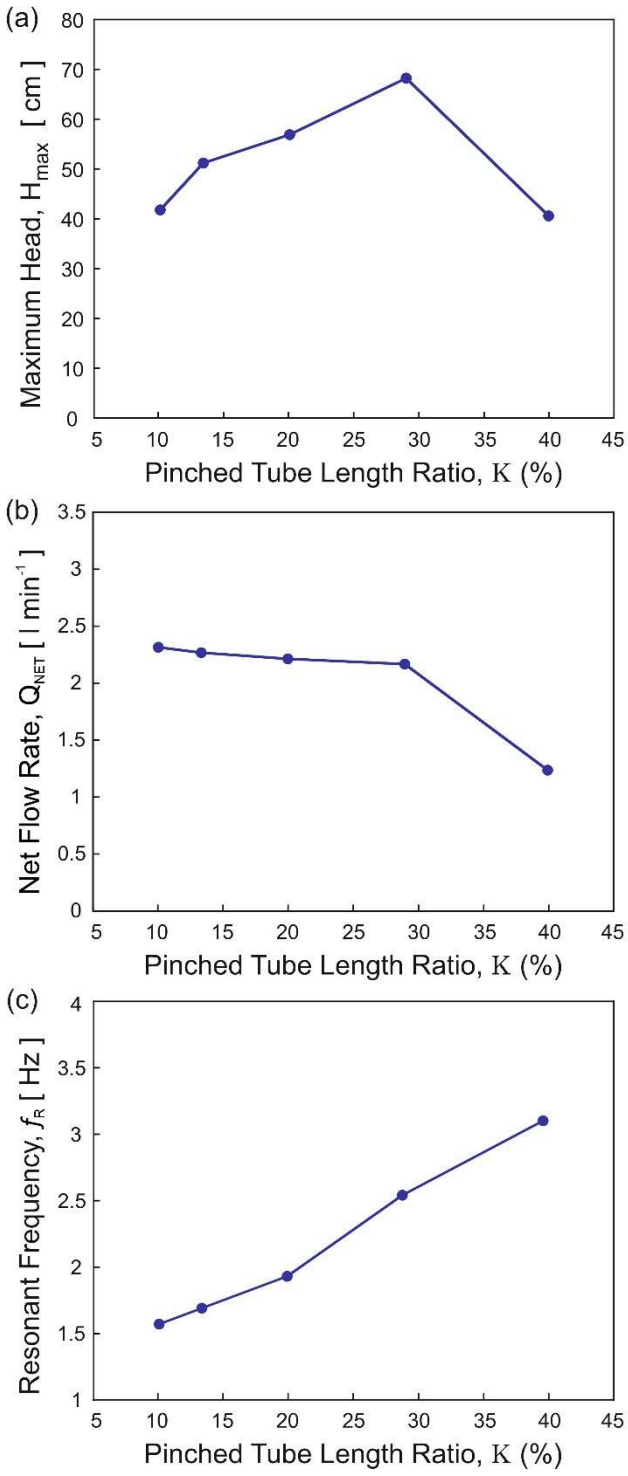

Figure 13. (a) The maximum head in an unsteady test, (b) the net flow rate in a steady test, and (c) the resonant frequency in a steady test for the pinched tube length ratio (K) (under nominal conditions).

F. Suitability of the proposed pump for biomedical applications

As noted by Loumes and Gharib[14], Liebau pumps possess several notable features that are particularly well-suited to a variety of biomedical applications. They have a simple and compact design and lack components such as blades or valves that might affect the biofluid. In addition to their potential use as an intra-aortic assist device[31], they may also be suitable for pediatric

extracorporeal membrane oxygenation (ECMO) and as paracorporeal or extracorporeal ventricle assist devices (VAD) for infants. Figure 14 compares the experimental data for the soft robotic pump developed within this study under nominal conditions and with two different values of the length ratio (λ) with the reference ranges for pediatric ECMO treatment[32] and VAD[33,34]. The VAD area is obtained considering a body mass of up to 20 kg and a range of actuation between 2 and 16 mmHg[34]. Figure 14 shows that the pump curves cross the lower range of the pressure and flow rates for ECMO and the full region for VAD. This result implies that a combination of these pumps could make them adequate for the requirements of a higher head.

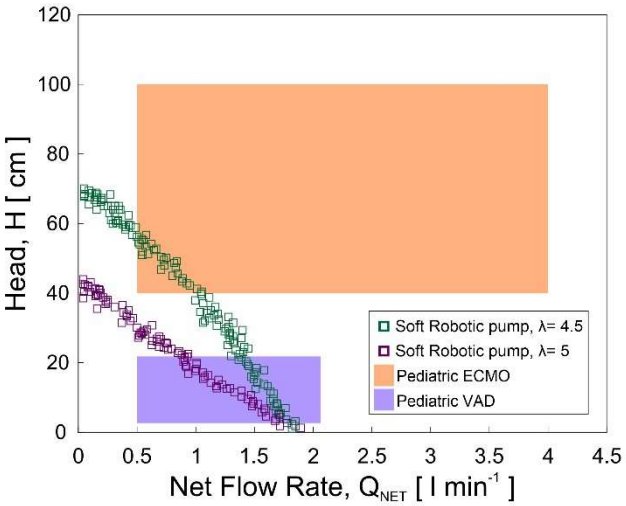

Figure 14. Pediatric ECMO and VAD application ranges overlaid on the soft robotic pump characteristic curves for λ= 4.5 and λ= 5 under nominal conditions.

Furthermore, given recent advances in multipincher Liebau pumps[35], it is expected that the range of operation of these pumps will extend in the near future, making it possible to use them in more biomedical applications, such as plasmapheresis, dialysis, and microfluidic devices working with blood.

IV. Conclusion

In this paper, an asymmetric pump based on a soft robotic pincher has been developed and tested experimentally. The production process has been described in detail, along with the main operating conditions and performance of the pump. A detailed performance analysis and a parametric study were carried out to describe the asymmetric. The findings of this study offer evidence of the importance of the pinching frequency and its alignment with the natural frequency of the pump. In addition, the performance of the new pump proposed here has been quantified from first principles and shows a much better efficiency than previous valveless designs. One can conclude from these results that soft-robotics pinchers are very suitable for valveless pumping in different areas involving the pumping of special fluids, such as biomedical applications.

ACKNOWLEDGMENTS

The authors would like to thank the Junta de Castilla y León for funding this work as part of the program "Subvenciones del programa de apoyo a proyectos de investigación financiados por fondos FEDER" under project number VA182P20.

AUTHORS DECLARATIONS

Conflict of interest

The authors have no conflicts to disclose.

Authors contributions

J. Anatol: Conceptualization, Methodology, Investigation, Data Curation, Writing – Original Draft. **M. García-Díaz:** Conceptualization, Formal analysis, Investigation, Resources, Writing – Original Draft. **C. Barrios-Collado:** Methodology, Validation, Investigation, Data Curation, Writing – Original Draft. **J. A. Moneo-Fernández:** Software, Validation, Resources. **F. Castro-Ruiz:** Conceptualization, Methodology, Investigation, Writing – Review & Editing, Visualization, Project administration. **J. Sierra-Pallares:** Formal analysis, Investigation, Writing – Review & Editing, Supervision, Funding acquisition.

DATA AVAILABILITY

The data that support the findings of this study are available from the corresponding author upon reasonable request.

Nomenclature

a	Width of the pinching region
c_P	Specific heat at constant pressure
D	Diameter of the pneumatic piston
D_1	Inner diameter of rigid pipe 1
D_2	Inner diameter of rigid pipe 2
D_3	Inner diameter of the compliant tube
D_4	Inner diameter of the soft robot
f	Frequency
f_R	Resonant frequency
F1	Flowmeter in position 1
F2	Flowmeter in position 2
F3	Flowmeter in position 3
F4	Flowmeter in position 4
g	Acceleration of gravity
h	Specific enthalpy

h_1	Height of water in Reservoir 1
h_2	Height of water in Reservoir 2
H	Head
H_{MAX}	Maximum head
$\mathcal{H}$	Enthalpy
ℓ_2	Length of the soft robot inner chamber
L	Length between reservoirs
L_1	Length between Reservoir 1 and pinching region
L_2	Length between Reservoir 2 and pinching region
L_3	Length of the compliant tube
m	Mass
P	Absolute supply pressure
P_0	Absolute initial pressure
P1	Pressure meter in rigid pipe 1
P2	Pressure meter in rigid pipe 2
Pd	Pressure meter in Reservoir 2
PO	Pincher open
PC	Pincher closed
P_t	Operating pressure
Q	Flow rate
Q_1	Flow rate in rigid pipe 1
Q_2	Flow rate in rigid pipe 2
Q_{NET}	Net flow rate
r	Vessel radius
R	Specific gas constant
S	Stroke of the piston
t	Time
T	Cycle period
V_0	Initial volume of air
wt	Wall thickness of the compliant tube
W	Pumping power

Wd	Drive power
Wo	Womersley number
Greek Symbols	
μ	Viscosity of the fluid
ρ	Density of the fluid
η	Efficiency
K	Pinched tube length ratio, a/L_3
λ	Length ratio, L_2/L_1
θ	Temperature

REFERENCES

[1] T. Kenner, M. Moser, I. Tanev, and K. Ono, "The Liebau-effect or on the optimal use of energy for the circulation of blood," Scripta Medica Facultatis Medicae Universitatis Brunensis Masarykianae **73**(1), 9–14 (2000).

[2] G. Liebau, "On a valveless pump principle (ger)," Naturwissenschaften **327**, 1 (1954).

[3] T. Kenner, *Biological Asymmetry and Cardiovascular Blood Transport* (Universität Graz/Technische Universität Graz. SFB F003 - Optimierung und Kontrolle, Graz, 2004).

[4] J. Anatol, M. García-Díaz, C. Barrios-Collado, J.A. Moneo-Fernández, M. Horvath, T. Parra, F. Castro-Ruiz, E.T. Roche, and J. Sierra-Pallares, "Experimental study of an asymmetric valveless pump to elucidate insights into strategies for pediatric extravascular flow augmentation," Scientific Reports **12**(1), 22165 (2022).

[5] T.T. Bringley, S. Childress, N. Vandenberghe, and J. Zhang, "An experimental investigation and a simple model of a valveless pump," Physics of Fluids **20**(3), 033602 (2008).

[6] A.I. Hickerson, and M. Gharib, "On the resonance of a pliant tube as a mechanism for valveless pumping," Journal of Fluid Mechanics **555**, 141 (2006).

[7] S. Timmermann, and J.T. Ottesen, "Novel characteristics of valveless pumping," Physics of Fluids **21**(5), 053601 (2009).

[8] C.-Y. Wen, and H.-T. Chang, "Design and Characterization of Valveless Impedance Pumps," **25**(4), 345–354 (2009).

[9] C.G. Manopoulos, D.S. Mathioulakis, and S.G. Tsangaris, "One-dimensional model of valveless pumping in a closed loop and a numerical solution," Physics of Fluids **18**(1), 017106 (2006).

[10] N. Sarvazyan, "Building valveless impedance pumps from biological components: Progress and challenges," Frontiers in Physiology **12**(January), 770906 (2021).

[11] C. Manopoulos, S. Tsangaris, and D. Mathioulakis, "Net flow generation in closed-loop valveless pumping," Proceedings of the Institution of Mechanical Engineers, Part C: Journal of Mechanical Engineering Science **234**(11), 2126–2142 (2020).

[12] K. Kounanis, and D.S. Mathioulakis, "EXPERIMENTAL FLOW STUDY WITHIN A SELF OSCILLATING COLLAPSIBLE TUBE," **13**(1), 61–73 (1999).

[13] D. Yiasemides, An. Argyris, and D.S. Mathioulakis, "Transitory and Periodic Flow in a Self-Oscillating Collapsible Tube: Experimental Study," **143**(4), 1–11 (2017).

[14] L. Loumes, I. Avrahami, and M. Gharib, "Resonant pumping in a multilayer impedance pump," Physics of Fluids **20**(2), 023103 (2008).

[15] K. Kumar, and D. Prabhakaran, "Nonlinear oscillations of a collapsible tube subjected to unsteady external pressure," Physics of Fluids **34**(6), 061907 (2022).
[16] W. Dai, S.L. Hale, and R.A. Kloner, "Cardiac cells implanted within the outer aortic wall of rats generate measurable contractile force," Regenerative Medicine **1**(1), 119–124 (2006).
[17] N. Sarvazyan, "Thinking outside the heart: Use of engineered cardiac tissue for the treatment of chronic deep venous insufficiency," **19**(4), 394–401 (2014).
[18] C.-Y. Wen, S.-J. Yeh, K.-P. Leong, W.-S. Kuo, and H. Lin, "Application of a Valveless Impedance Pump in a Liquid Cooling System," **3**(5), 783–791 (2013).
[19] J.A. Meier, *A Novel Experimental Study of a Valveless Impedance Pump for Applications at Lab-On-Chip, Microfluidic, and Biomedical Device Size Scales* (2011).
[20] Z. Li, Y. Seo, O. Aydin, M. Elhebeary, R.D. Kamm, H. Kong, and M.T.A. Saif, "Biohybrid valveless pump-bot powered by engineered skeletal muscle," Proceedings of the National Academy of Sciences of the United States of America **116**(5), 1543–1548 (2019).
[21] H. Azizgolshani, and M. Gharib, *Tissue Engineering Active Biological Machines* (California Institute of Technology, Pasadena, California, 2013).
[22] S. TAKAGI, and T. SAIJO, "Study of a Piston Pump without Valves: 1st Report, On a Pipe-capacity-system with a T-junction," Bulletin of JSME **26**(218), 1366–1372 (1983).
[23] S. TAKAGI, and K. TAKAHASHI, "Study of a Piston Pump without Valves: 2nd Report, Pumping Effect and Resonance in a Pipe-capacity-system with a T-junction," Bulletin of JSME **28**(239), 831–836 (1985).
[24] G. Propst, "Pumping effects in models of periodically forced flow configurations," Physica D: Nonlinear Phenomena **217**(2), 193–201 (2006).
[25] I. Avrahami, and M. Gharib, "Computational studies of resonance wave pumping in compliant tubes," Journal of Fluid Mechanics **608**, 139–160 (2008).
[26] Jung, Eunok, and Kim, Do Wan, "Valveless pumping in open tank system using energy conserving compartment model," Bulletin of the Korean Mathematical Society **49**(5), 961–987 (2012).
[27] E.T. Roche, M.A. Horvath, I. Wamala, A. Alazmani, S.-E. Song, W. Whyte, Z. Machaidze, C.J. Payne, J.C. Weaver, G. Fishbein, J. Kuebler, N.V. Vasilyev, D.J. Mooney, F.A. Pigula, and C.J. Walsh, "Soft robotic sleeve supports heart function," Science Translational Medicine **9**(373), (2017).
[28] C. Park, Y. Fan, G. Hager, H. Yuk, M. Singh, A. Rojas, A. Hameed, M. Saeed, N.V. Vasilyev, T.W.J. Steele, X. Zhao, C.T. Nguyen, and E.T. Roche, "An organosynthetic dynamic heart model with enhanced biomimicry guided by cardiac diffusion tensor imaging," Sci. Robot. **5**(38), eaay9106 (2020).
[29] W. Chen, H. Zheng, Z. Yan, and R. Chen, "Shape design of an artificial pump-lung using high-resolution hemodynamic simulation with high-performance computing," Physics of Fluids **35**(3), 031909 (2023).
[30] A.I. Hickerson, D. Rinderknecht, and M. Gharib, "Experimental study of the behavior of a valveless impedance pump," Experiments in Fluids **38**(4), 534–540 (2005).
[31] J. Litmathe, U. Boeken, P. Feindt, R. Marktanner, and E. Gams, in *Transplantation Proceedings* (Elsevier, 2004), pp. 3123–3128.
[32] S. Takatani, H. Hoshi, K. Tajima, K. Ohuchi, M. Nakamura, J. Asama, T. Shimshi, and M. Yoshikawa, "Feasibility of a Miniature Centrifugal Rotary Blood Pump for Low-Flow Circulation in Children and Infants," ASAIO Journal **51**(5), 557 (2005).
[33] K. Puri, and I. Adachi, in *Seminars in Thoracic and Cardiovascular Surgery: Pediatric Cardiac Surgery Annual* (Elsevier, 2021), pp. 10–18.
[34] E. Buratto, X.T. Ye, G. King, W.Y. Shi, R.G. Weintraub, Y. d'Udekem, C.P. Brizard, and I.E. Konstantinov, "Long-term outcomes of single-ventricle palliation for unbalanced atrioventricular septal defects: Fontan survivors do better than previously thought," The Journal of Thoracic and Cardiovascular Surgery **153**(2), 430–438 (2017).

[35] M. Rosenfeld, and I. Avrahami, “Net flow rate generation by a multi-pincher impedance pump,” Computers and Fluids **39**(9), 1634–1643 (2010).